2nd NOAA AI Workshop 18th Feb, 2021

Deep learning based precipitation retrieval algorithm using passive microwave observations

PMW-PrecipNet

Yeji Choi(yejichoi@si-analytics.ai)
AI Research team, SI Analytics

Collaborators: Seongchan Kim[1], Guohua Li[1],
Jeongmyeong Choi[2], Jaemin Jeong[2],
Ji-Hye Kim[3],
Dong-Bin Shin[4]

1 KiSTi Korea Institute of Science and Technology Information www.kisti.re.kr
2 한림대학교 HALLYM UNIVERSITY
3 KOREA UNIVERSITY
4 YONSEI UNIVERSITY

SIA SI ANALYTICS

SIA SI ANALYTICS **Partners**

Ministry of the Interior and Safety National Disaster Management Research Institute

KARI Korea Aerospace Research Institute

책임운영기관 National Institute of Meteorological Sciences

Agency for Defense Development

SI

SIIS

NVIDIA.

GEOINT Analysis

Detect and classify
the types of objects and land covers.

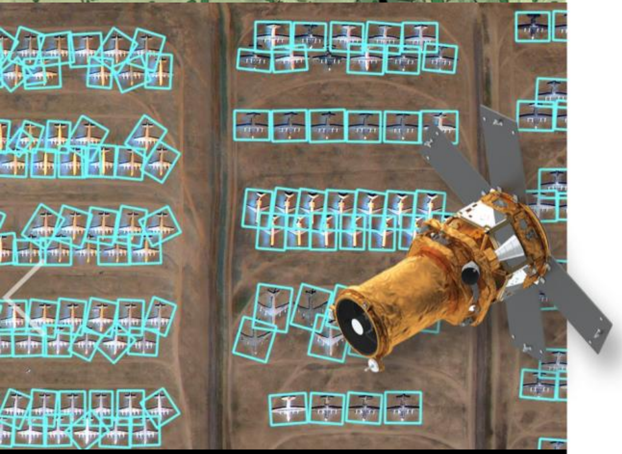

Defense & Intelligence

Superior geospatial intelligence, surveillance
to solve national security and challenges.

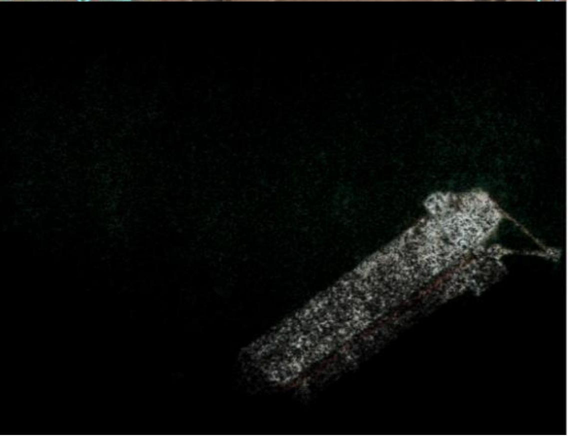

eXplainable-AI (XAI)

Explainable artificial intelligence for satellite/aerial imagery

- **Object Detection**- Artificial intelligence to automatically detect major objects of interest in the satellite imagery- Result analysis such as object size and type
- **eXplainable AI (XAI)**- Explainable artificial intelligence for the reliability of analysis results- Reliability verification of object analysis results by explainable AI
- **Semantic Segmentation**- Semantic segmentation for analysis of topography shape, type, and features- Smart land-use analysis by terrain features
- **Super Resolution**- Increasing resolution of satellite imagery using artificial intelligence- Performance improvement of analysis technology by applying super resolution technology
- **Change Detection**- Technology for automatically detecting changed areas and objects using artificial intelligence- Detecting changes of terrain, buildings, roads, etc. and analyzing the extent and types of changes automatically

yejichoi@si-analytics.ai

Contents

- Motivation: Deep learning + meteorological satellite
- Rain-type segmentation (with Seongchan Kim)
  - RTC-U-net
  - RTC-fcNN
- Precipitation retrieval results (with Jeongmyeong Choi, Jaemin Jeong, Ji-Hye Kim)
  - PMW-PrecipNet
- Precipitation forecasting (on going…) (with Guohua Li)

yejichoi@si-analytics.ai

01 Motivations

yejichoi@si-analytics.ai

Deep learning + meteorological satellite data

PERSPECTIVE

https://doi.org/10.1038/s41586-019-0912-1

Deep learning and process understanding for data-driven Earth system science

Markus Reichstein[1,2*], Gustau Camps-Valls[3], Bjorn Stevens[4], Martin Jung[1], Joachim Denzler[2,5], Nuno Carvalhais[1,6] & Prabhat[7]

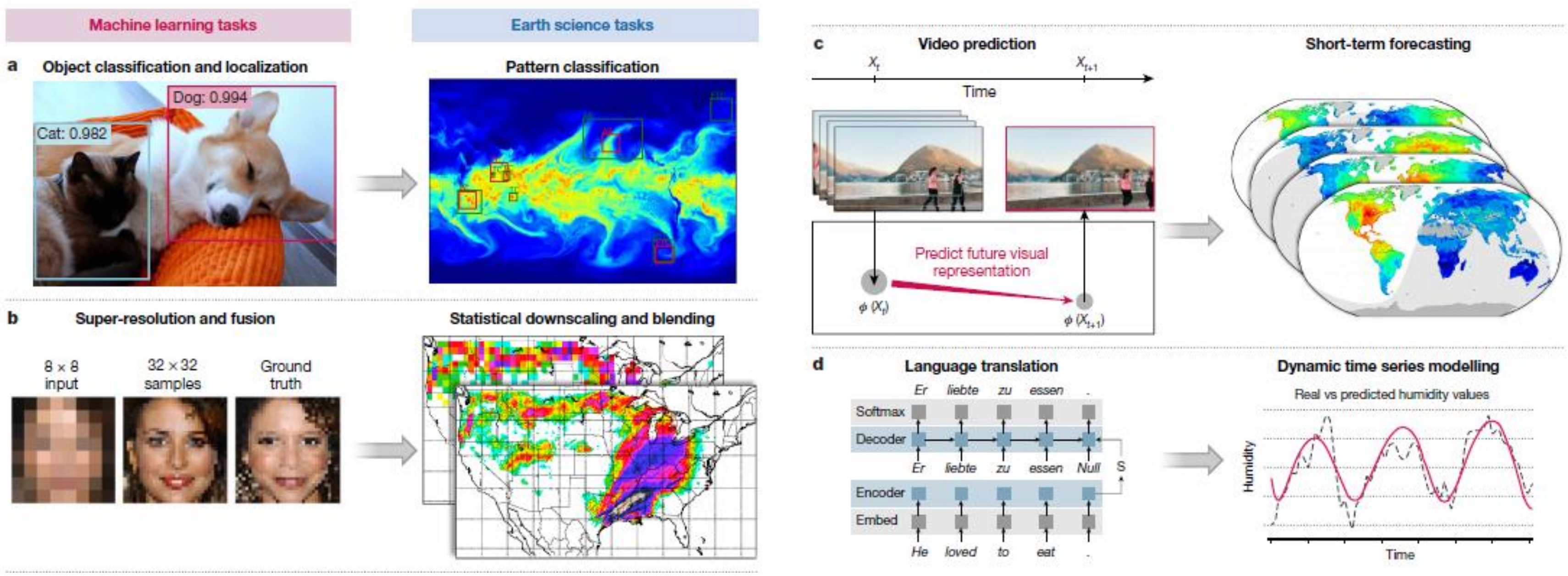

NOAA Data Volume graph, Courtesy Steve Del Greco & Ken Casey, NOAA/ NCEI (via Jeff de La Beaujardiere), 2016

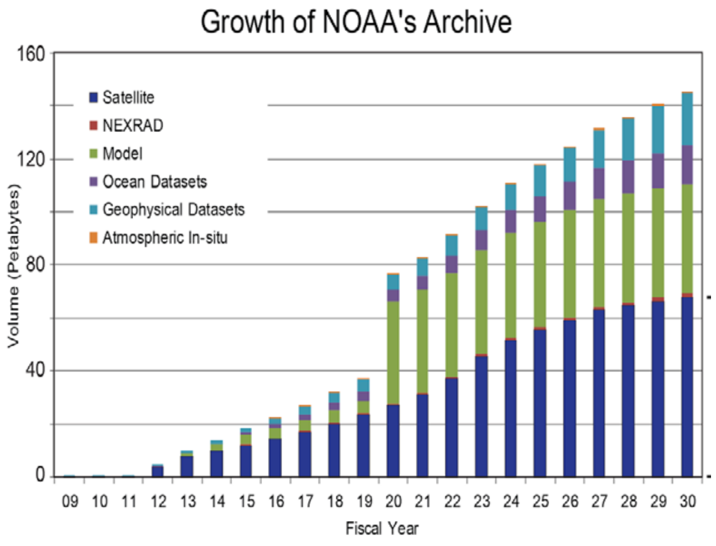

Motivation

Accurate measurements of precipitation are important
not only for weather and climate scientist,
but also for a wide range of decision makers,
including hydrologists, agriculturalists, and emergency managers.

History

Precipitation retrievals from space

From a experimental stage of remote sensing with microwave, rainfall measurements is one of the major subject to research.

ESMR
(electrically scanned MW radiometer)
1972~1983
✓19GHz (Nimbus-5)
✓37GHz(Nimbus-6)
✓Resolution :25km

SMMR
(scanning multichannel MW radiometer) 1978~1994
✓6.6,10.7,
18, 21, 37GHz
✓Resolution : 30~155km

SSM/I->SSMIS
(Special Sensor MW/ Imager(Sounder))
1987~pres.
✓SSM/I (GHz): 19.35, 22.2(V), 37, 85.5(H/V)
✓SSMIS (GHz): SSM/I+50.2(H), 52.8(H), 53.596(H), 54.4(H), 55.5(H), 91.7(V/H), 150(H), Sounding Channels
✓Resolution : 12.5~25km

TMI 1997~2014
(TRMM microwave imager)
✓10, 19, 21(V), 37, 85 GHz (H/V)
✓Resolution :7~50km

AMSU 1998~pres.
(Advanced Microwave sounding Unit)
✓A : 23.8~89 GHz-15ch
✓B : 89~183 GHz -5ch
✓Resolution : 15~45km

AMSR-E(AMSR2)
(Advanced microwave scanning radiometer)
2002~2011/2012~
✓6.925, 7.3, 10.65, 18.7, 23.8, 36.5, 89.0 GHz
✓Resolution : 4~43km

GMI
(Global precipitation Measurement)
2014~pres.
✓10.65, 18.70, 23.8, 36.5, 89.0, 166, 183 GHz
✓Resolution : 5~25km

ATMS
(Advanced Technology Microwave Sounder)
2011~pres.
✓23.8~183.31 GHz –21ch
✓Resolution : 15.8~74.8km

MADRAS
(Microwave Analysis & Detection of Rain & Atmospheric Structures)
2011~pres.
✓18.7, 23.8(V), 36.5, 89.0, 157.0 (H/V) GHz
✓Resolution : 15.8~74.8km

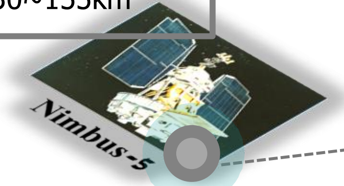

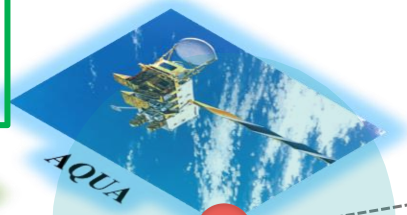

1970's
Experimental stage

1980's
Operational use

1990's
The first space radar
Toward higher resolutions

2000's

2010's

SIA

Global precipitation measurements (GPM)

The Global Precipitation Measurement (GPM) mission is an international network of satellites that provide next-generation global observations of rain and snow. (initiated by NASA and JAXA)

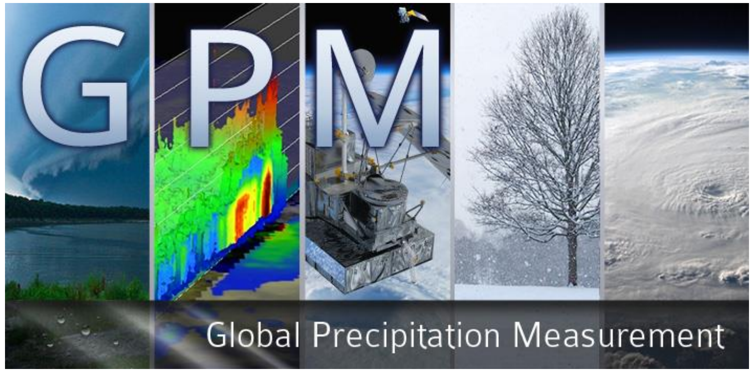

GPM Constellation Status

Reference satellite
with DPR (radar sensors)

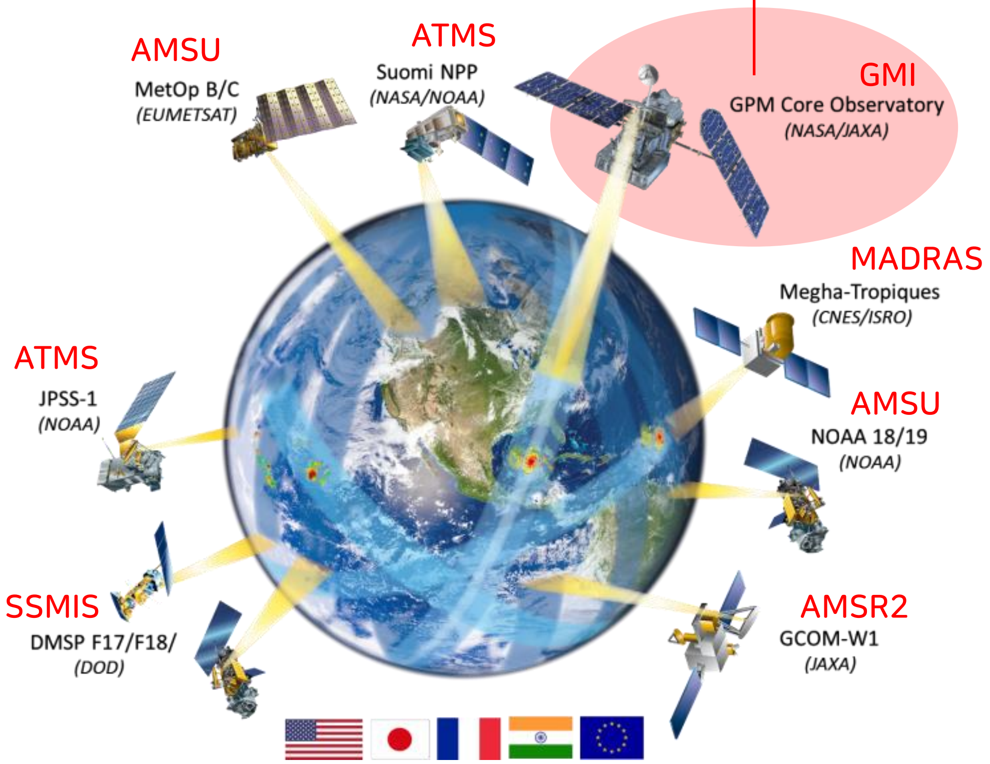

IMERG products: every 30 min global precipitation measurements

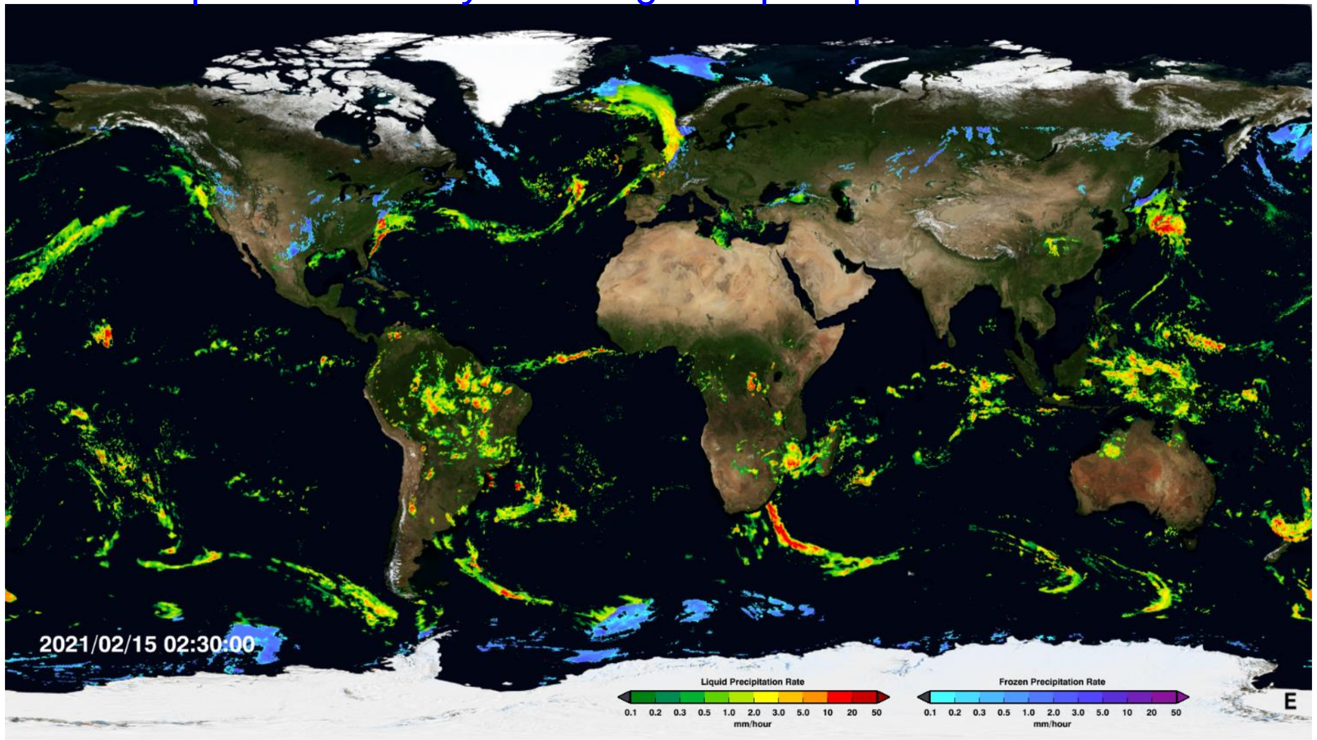

Yonsei’s precipitation retrieval algorithm

Choi, Yeji, Dong-Bin Shin, and Minsu Joh. "Assessment of WRF microphysics schemes in simulation of extreme precipitation events based on microwave radiative signatures." *International Journal of Remote Sensing* 39.23 (2018): 8527-8551.
Choi, Yeji, et al. "Passive Microwave Precipitation Retrieval Algorithm With A~ Priori Databases of Various Cloud Microphysics Schemes: Tropical Cyclone Applications." *IEEE Transactions on Geoscience and Remote Sensing* 58.4 (2019): 2366-2382.

[Bayesian Inversion Method]

$$P(\mathbf{R}\,|\,\mathbf{T_b}) \propto P(\mathbf{R}) \times P(\mathbf{T_b}\,|\,\mathbf{R})$$

The probability of a certain rain rate, R, from CRM

The probability of observing the TBs given the rain rate from RTM

[Constructing a-priori database]

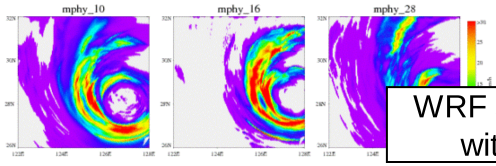

WRF simulation with **MP8** | WRF simulation with **MP10** | WRF simulation with **MP16** | WRF simulation with **MP17** | WRF simulation with **MP28**

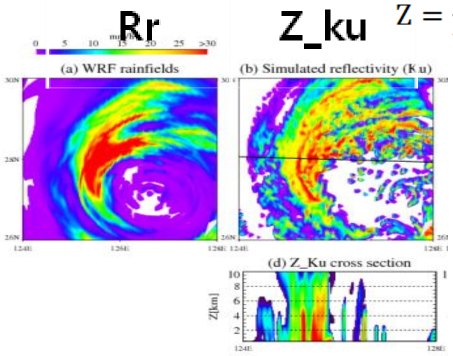

$$Z = \frac{\lambda^4}{\pi^5 |K|^2} \int_D \sigma_b(D) N(D) dD$$

Calculation of Z profiles
with hydrometeor profiles

TRMM PR observation

Matching Z profiles
over PR/DPR scan swath

3-D precipitation fields over PR scan strips

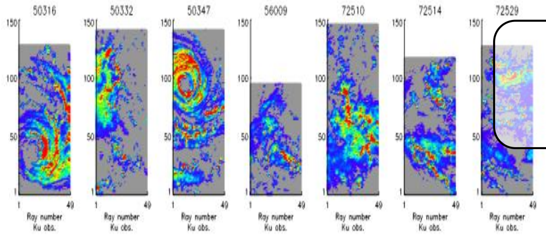

Yonsei's precipitation retrieval algorithm

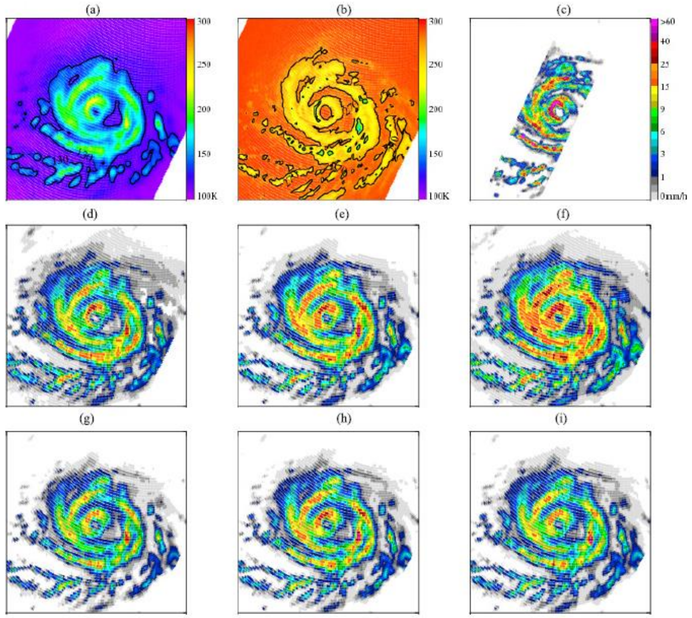

Fig. 10. Retrieval results for Typhoon Soudelor (orbit number: 8158) depending on five different microphysics schemes. (a) Emission and (b) scattering signatures from GPM GMI sensor. (c) Averaged rain rate from GPM DPR for targeted orbits. (d) GPROF rain rate. (e)–(i) Precipitation retrieval results obtained with various *a priori* databases. (a) 10H_TB (1BGNI). (b) PCT89 (1BGMI). (c) PR (2ADPR). (d) GPROF. (e) MP8. (f) MP10. (g) MP16. (h) MP17. (i) MP28.

Choi, Yeji, Dong-Bin Shin, and Minsu Joh. "Assessment of WRF microphysics schemes in simulation of extreme precipitation events based on microwave radiative signatures." *International Journal of Remote Sensing* 39.23 (2018): 8527-8551.
Choi, Yeji, et al. "Passive Microwave Precipitation Retrieval Algorithm With A~ Priori Databases of Various Cloud Microphysics Schemes: Tropical Cyclone Applications." *IEEE Transactions on Geoscience and Remote Sensing* 58.4 (2019): 2366-2382.

✓ **TB-R relations depending on rain type**

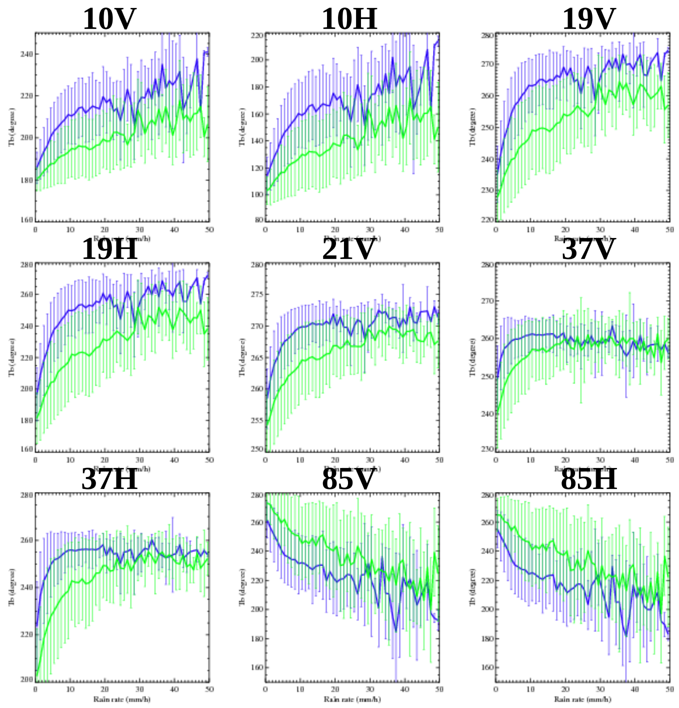

Stratiform
convective

➢ TB histogram depending on rain type

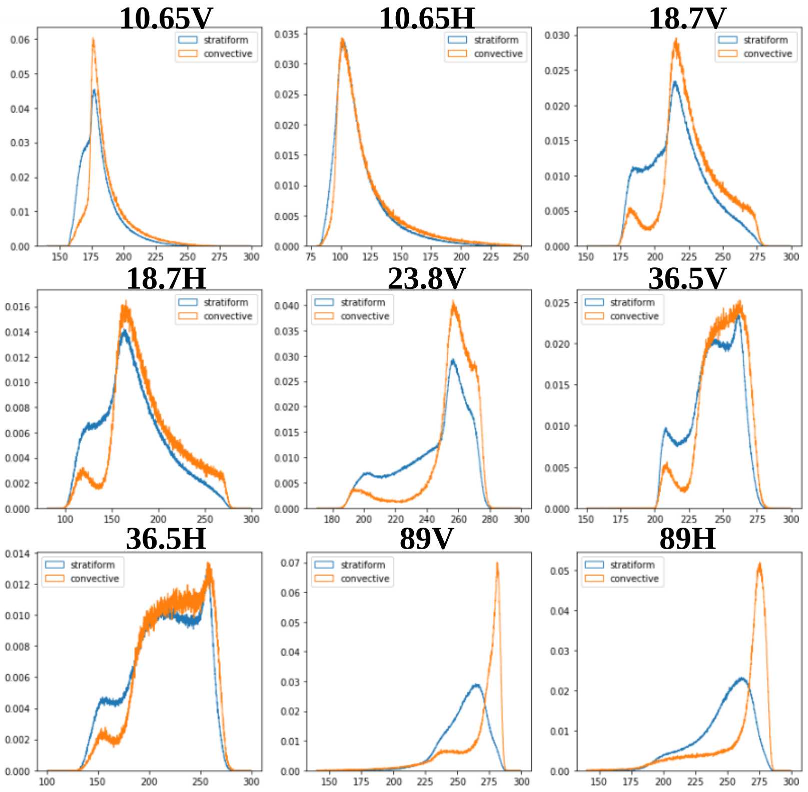

✓ **Emission and scattering relations**

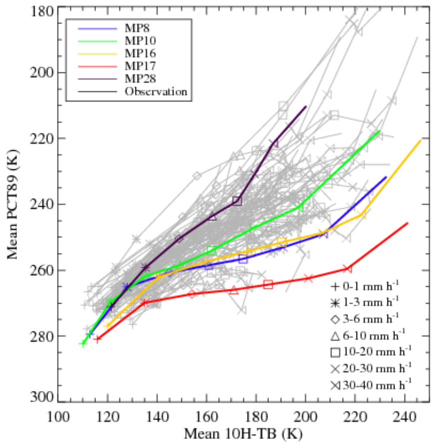

02 Rain-type segmentation

Choi, Yeji, and Seongchan Kim. "Rain-Type Classification From Microwave Satellite Observations Using Deep Neural Network Segmentation." *IEEE Geoscience and Remote Sensing Letters* (2020).

yejichoi@si-analytics.ai

Motivation

Convective and Stratiform

Separating convective and stratiform (C/S) precipitation types is very important for passive microwave rainfall retrievals.

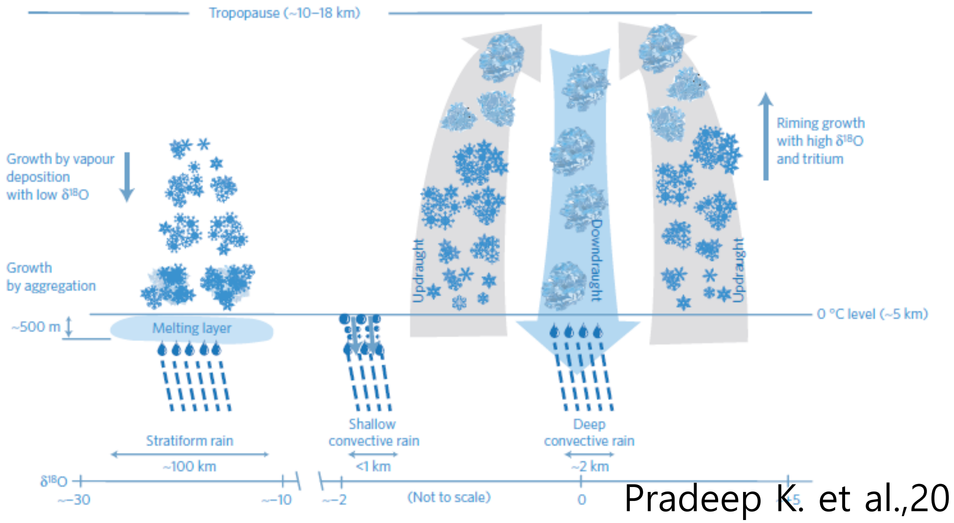

Pradeep K. et al.,2016

Figure 2 | Schematic representation of differences in dynamical and microphysical processes in convective and stratiform precipitation resulting in isotope variations. (Adapted after refs 18,19.) The upward air motion above the 0 °C level is ~5–10 m s^{-1} in convective updraughts and ~0.2 m s^{-1} in stratiform clouds. Hydrometeors in convective clouds grow as they are lifted in updraughts, while in stratiform clouds, they grow as they fall slowly towards the surface.

- ✓ C/S separation algorithm using the combination of 19, 37, 85 GHz data (Hong et al., 1999)
- ✓ Precipitation type classification method using 37GHz observations (Jiang et al., 2018)
- ✓ Using AdaBboost (Adaptive boosting algorithm) and LDA (Linear discriminant analysis)- Machine Learning Technique (T.Islam et al., 2015)
- ✓ Using deep learning technique-fully connected neural network (V. Petkovi´c et al., 2019)

Stratiform	Convective
- Vertical air motions are weak (mean upward air velocity:~0.2m/s) - Below the freezing level, melting occurs in an ~500m thick layer. - Relatively small rain drops (D~1mm) - Hundreds of kilometers in scale	- Strong updraft (1~10m/s) - Melt rapidly below the 0°C - Large raindrops (D>2mm) - A few km to about 30 km in scale

Dataset preparation

- 2016.01~ 2018.12 (# of data:~17,000 (6TB))
- subset : Region(120E-175E/5N-55N), 40*40,
  # of data: 59,210

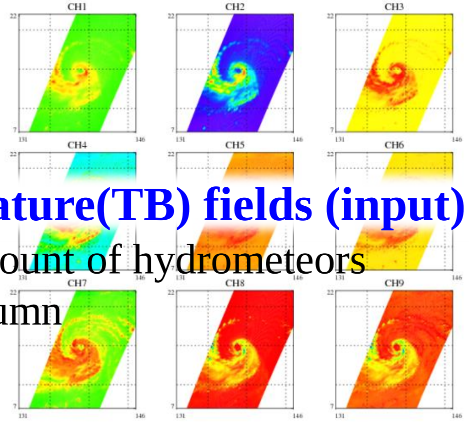

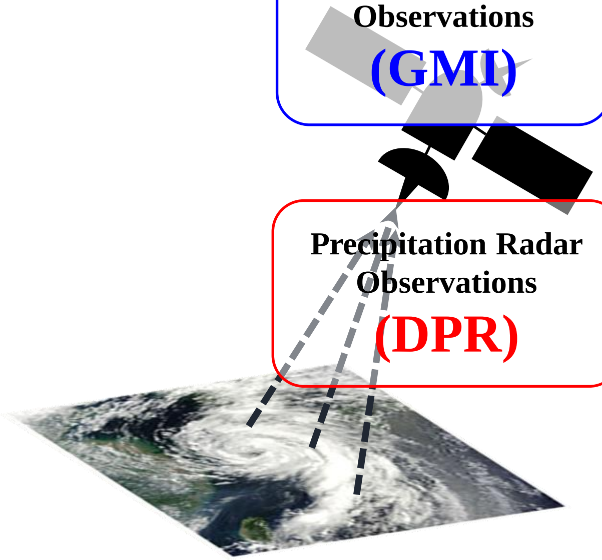

Passive microwave Observations (GMI)

Brightness temperature(TB) fields (input)

related to the gross amount of hydrometeors in the vertical rain column

Precipitation Radar Observations (DPR)

Rain type from Radar reflectivity (label)

related to the accurate vertical structures of precipitating system

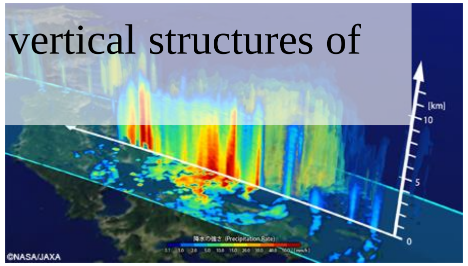

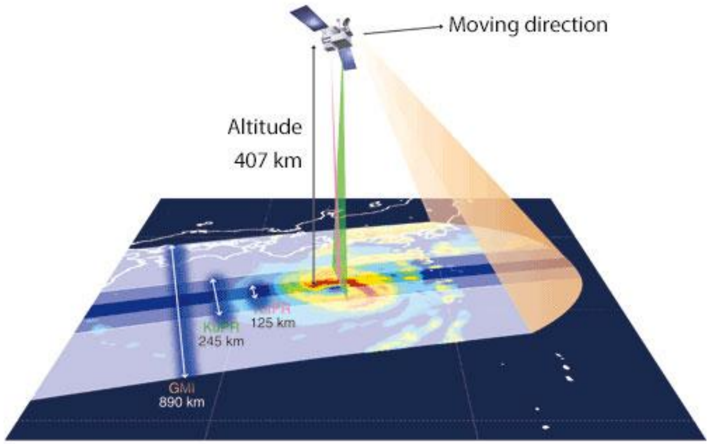

➢ GPM observation

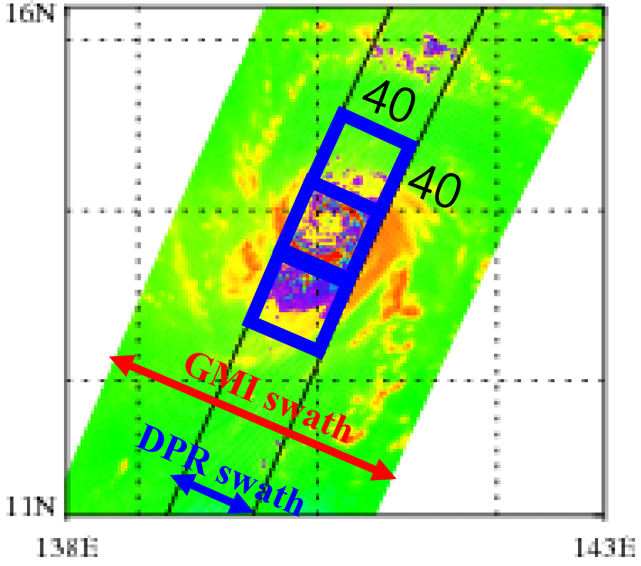

Input(n, 40,40,10)
: TBs for 9 channels, surface type
Label(n)
: Rain rate

Dataset preparation

GPM GMI Specification

channel	10.65 (H/V)	18.7 (H/V)	23.8 (V)	36.5 (H/V)	89.0 (H/V)	166 (H/V)	183.31 ±3(V)	183.31 ±7(V)
resolution	19.4 32.2	11.2 18.3	9.2 15.0	8.6 15.0	4.4 7.3	4.4 7.3	4.4 7.3	4.4 7.3
Sample NEDT (K)	0.96	0.84	1.05	0.65	0.57	1.5	1.5	1.5
Beam NEDT (K)	0.53	0.61	0.82	0.52	0.65	1.72	1.72	1.72
Incidence angle	Nominal Earth incidence=52.8° Off-nadir angle=48.5					Earth incidence=49.2° Off-nadir angle=45.4°		
Swath width	885km							
purpose	Liquid precip.	Moderate to light precip.	Water vapor emission	Moderate to light precip.	Detection of ice particle	Light precip.	Small ice particles and light rainfall and snowfall	

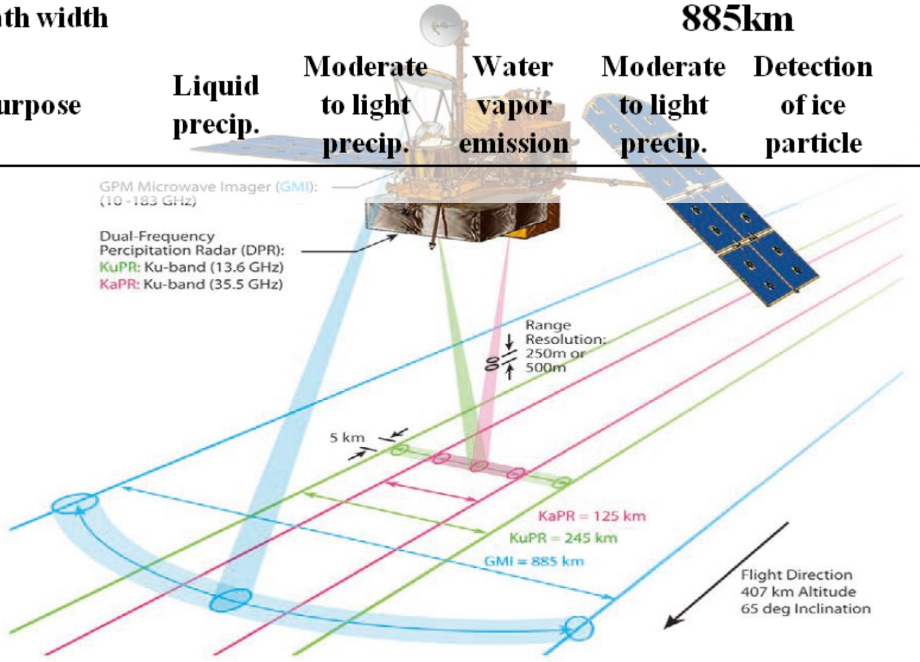

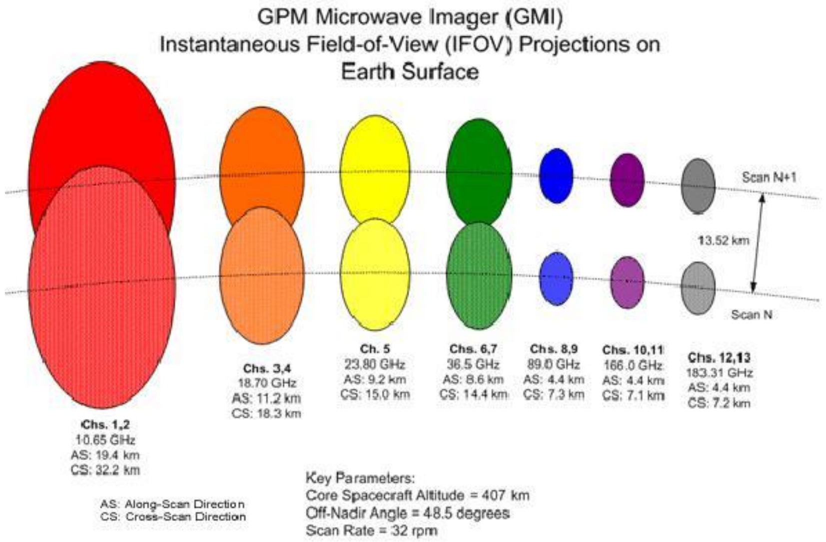

GPM DPR Specification

Instrument	GPM Ka-PR	GPM Ku-PR
Frequency (GHz)	35.5	13.6
Swath width (km)	120	245
Spatial resolution (km)	5.2	5.2
Range resolution (m)	250/500	250
Observation range (km)	18 to –3	18 to –5
Minimum detectable (dBz)	12 (0.2 mm/h)	18 (0.5 mm/h)
Measurement accuracy (dBZ)	<±1	<±1

Dataset

- 2016.01~ 2018.12 (# of data:~17,000 (6TB))
- subset : Region(120E-175E/5N-55N), 40*40,
  # of data: 59,210

TABLE I

RATIO OF EACH CLASS OF THE TRAINING DATA SET (NR: NO RAIN; ST: STRATIFOMR; CV: CONVECTIVE; AND OT: OTHER)

	Dataset	The # of image	NR(%)	ST(%)	CV(%)	OT(%)
More than 1 raining pixels	DATASET-I	46,239	90.76	6.25	2.23	0.76
over 10% of raining pixels	DATASET-II	11,465	72.05	21.38	4.61	1.96
over 50% of raining pixels	DATASET-III	1,410	44.65	48.52	4.51	2.31

Polarization corrected temperature

$$PCT10 = 2.5TB_{10V} - 1.5TB_{10H}$$

$$PCT19 = 2.4TB_{19V} - 1.4TB_{19H}$$

$$PCT37 = 2.15TB_{37V} - 1.15TB_{37H}$$

$$PCT89 = 1.7TB_{89V} - 0.7TB_{89H}$$

Original TBs from GMI observations

PCTs for 4 chs

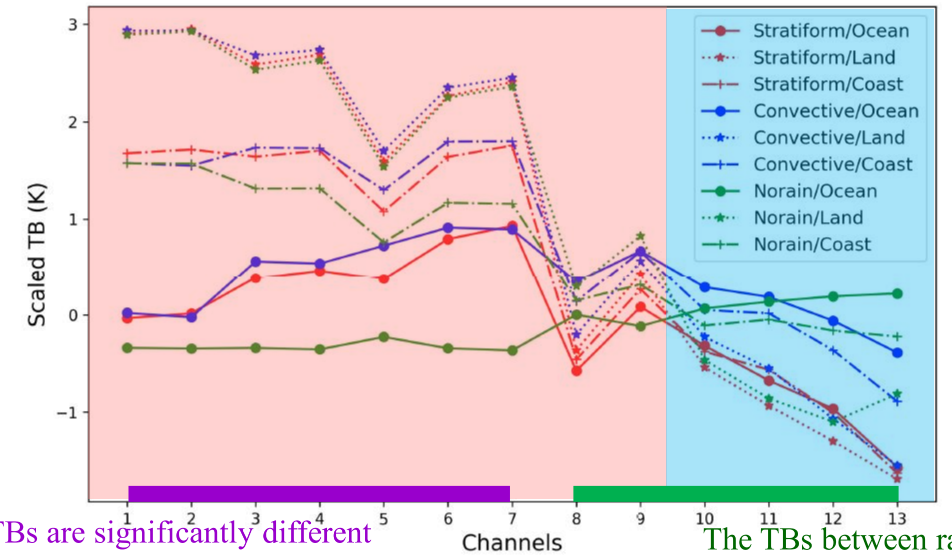

The TBs are significantly different depending on the surface types

The TBs between rain types at channels 8–13 are more distinguishable

Fig. 2. Mean normalized TBs at each channel depending on surface type.

DATA SET-I

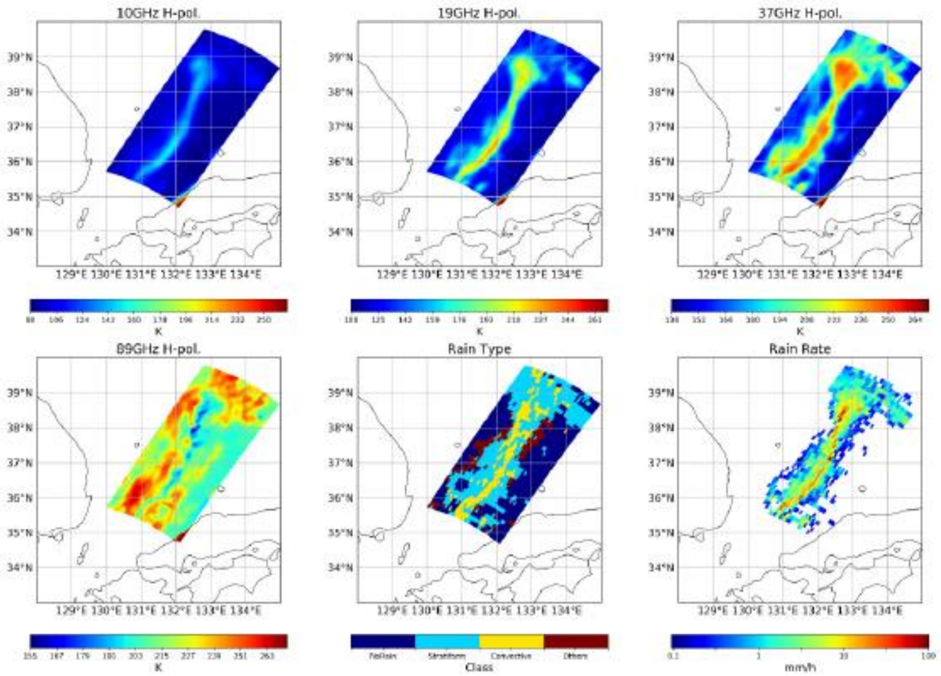

Fig. 1. Example of subset images of TBs (input) at 10-, 19-, 37-, and 89-GHz horizontally polarized channels from GMI observations, and rain types (label) and rain rate (referential information) from DPR observations (orbit number: 11371/2016.02.22).

Model architecture

We received the best model after 94 epoch, and it took 32.9 min for RTC-U-net.
For RTC-fcNN, the best model was obtained after 84 epoch (124.7 min).
We used four KIST NEURONs GPU system (NVIDIA Tesla V100 with NVLINK) for training.

➢ **RTC-U-net (convolutional networks)**

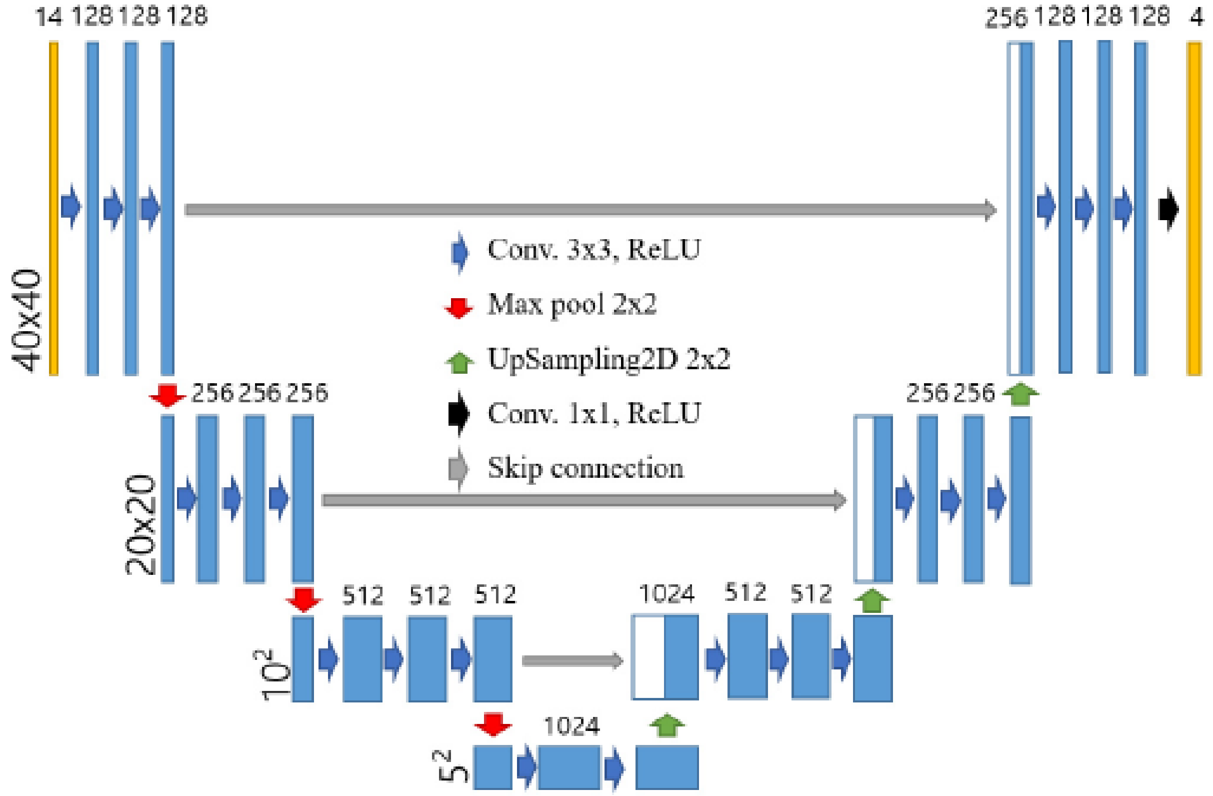

➢ **RTC-fcNN (Fully Connected Neural Network)**

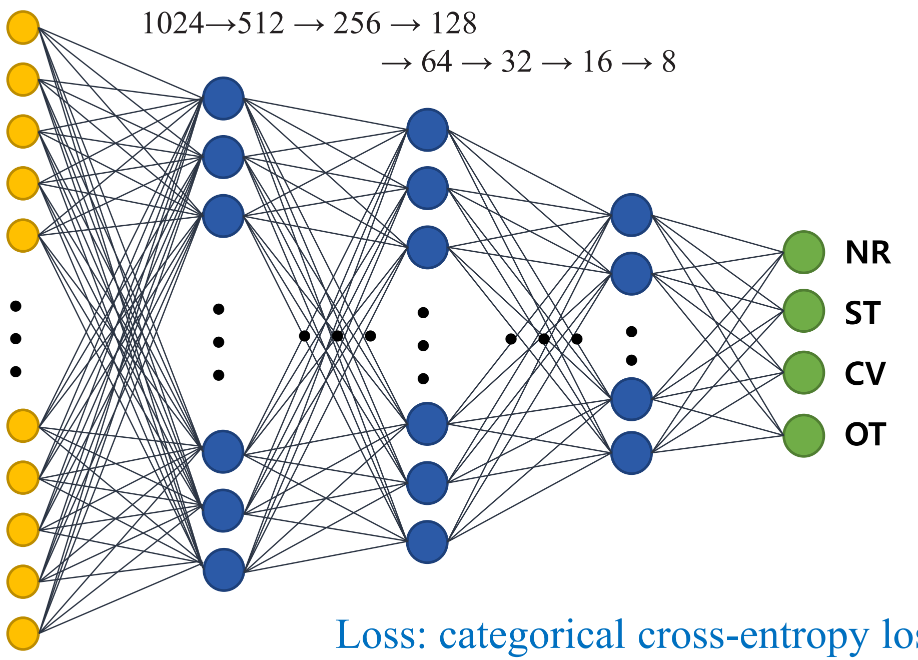

Loss: categorical cross-entropy loss
Activation: ReLU
Optimizer: Adam

Results

TABLE II

CLASSIFICATION RESULTS OF RTC-U-NET AND RTC-fcNN WITH PCT AND WITHOUT PCT (IN THE PARENTHESIS) (NR: NO RAIN; ST: STRATIFORM; CV: CONVECTIVE; AND OT: OTHER)

		Precision				Recall				F-score			
		NR	ST	CV	OT	NR	ST	CV	OT	NR	ST	CV	OT
RTC-U-net	DATASET-I	0.98(0.97)	0.79(0.83)	0.62(0.60)	0.53(0.52)	0.99 (0.99)	0.79(0.75)	0.40(0.44)	0.23(0.24)	0.98(0.98)	0.79(0.78)	0.49(0.51)	0.32(0.33)
	DATASET-II	0.97(0.97)	0.80(0.77)	0.60(0.62)	0.54(0.51)	0.99(0.99)	0.76(0.78)	0.36(0.34)	0.20(0.18)	0.98(0.98)	0.78(0.78)	0.45(0.44)	0.29(0.27)
	DATASET-III	0.95(0.95)	0.74(0.78)	0.65(0.62)	0.52(0.33)	0.99(0.99)	0.59(0.60)	0.01(0.06)	0.03(0.05)	0.97(0.97)	0.65(0.68)	0.02(0.10)	0.06(0.09)
RTC-fcNN	DATASET-I	0.97(0.97)	0.80(0.79)	0.58(0.60)	0.50(0.50)	0.99(0.99)	0.75(0.76)	0.37(0.34)	0.16(0.15)	0.98(0.98)	0.77(0.77)	0.45(0.43)	0.24(0.23)
	DATASET-II	0.97(0.97)	0.78(0.78)	0.58(0.58)	0.52(0.51)	0.99(0.99)	0.76(0.77)	0.38(0.37)	0.15(0.12)	0.98(0.98)	0.77(0.77)	0.46(0.45)	0.23(0.20)
	DATASET-III	0.96(0.96)	0.80(0.81)	0.54(0.54)	0.37(0.47)	0.99(0.99)	0.69(0.69)	0.16(0.19)	0.10(0.08)	0.98(0.98)	0.74(0.75)	0.25(0.28)	0.15(0.14)

Dataset	The # of image	NR(%)	ST(%)	CV(%)	OT(%)
DATASET-I	46,239	90.76	6.25	2.23	0.76
DATASET-II	11,465	72.05	21.38	4.61	1.96
DATASET-III	1,410	44.65	48.52	4.51	2.31

RTC-U-net, provides comparative results with the RTC-fcNN.
→ It shows the CNN technique is efficient to retrieve rain type for the entire image at once.
The scores of ST and CV shows a comparative result.
→ although the training data set has a dominant number of instances for the NR class.
The results with PCTs is similar despite significant PCT differences depending on rain type.
→ The PCTs are the linear combinations of TBs at two different channels, these linear relations is trained in the training process with only nine channels of observed TBs.
RTC-fcNN input: each pixel over an input image of RTC-U-net
→ The number of RTC-fcNN input data is multiplied with the number of pixels in the input image for RTC-U-net.
→ The results from RTC-fcNN with DATA SET-III are not significantly compromised with the reduced number of training data set.

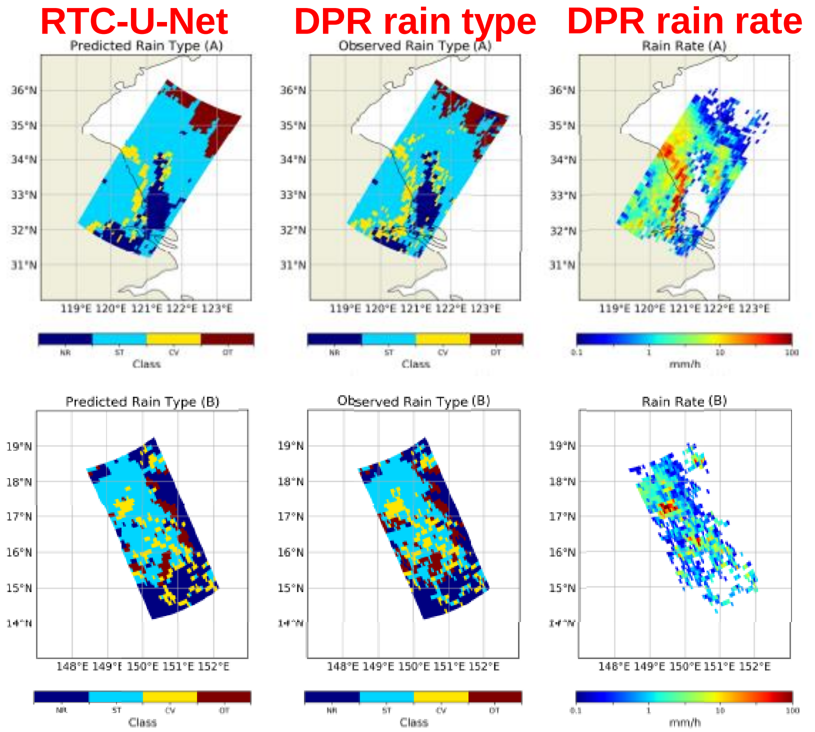

Conclusions

- We proposed two different DNNs: RTC U-net and RTC-fcNN, for rain type classification for all surface types.
- RTC U-net based on segmentation technique with CNN showed effective results. Moreover, the CV system's small cells are well distinguishable, although the ST system surrounds it.
- The RTC-fcNN with eight hidden layers showed a comparable performance although it has simple architectures. However, the training time is four times longer than RTC-U-Net.
- Rain type has highly imbalanced distributions, and NR usually has many more instances than the other classes. The results showed the accuracy is depending on the number of instances. We also checked the results with a balanced data set. However, there was a trade-off between missed detection and false alarm showing the missed detection was reduced while the false alarm was increased.
- Although PCTs are good criteria for raining areas and scattering signatures, we confirmed that the effect of PCTs as an input feature for DL is limited.

Using same data with rain type classification but using all 13 channels of GMI

03 Precipitation retrievals

PMW-PrecipNET: Precipitation retrieval based on Convolutional Neural Networks from passive microwave observations

yejichoi@si-analytics.ai

Model architecture

- U-Net based PMW-PrecipNET architecture

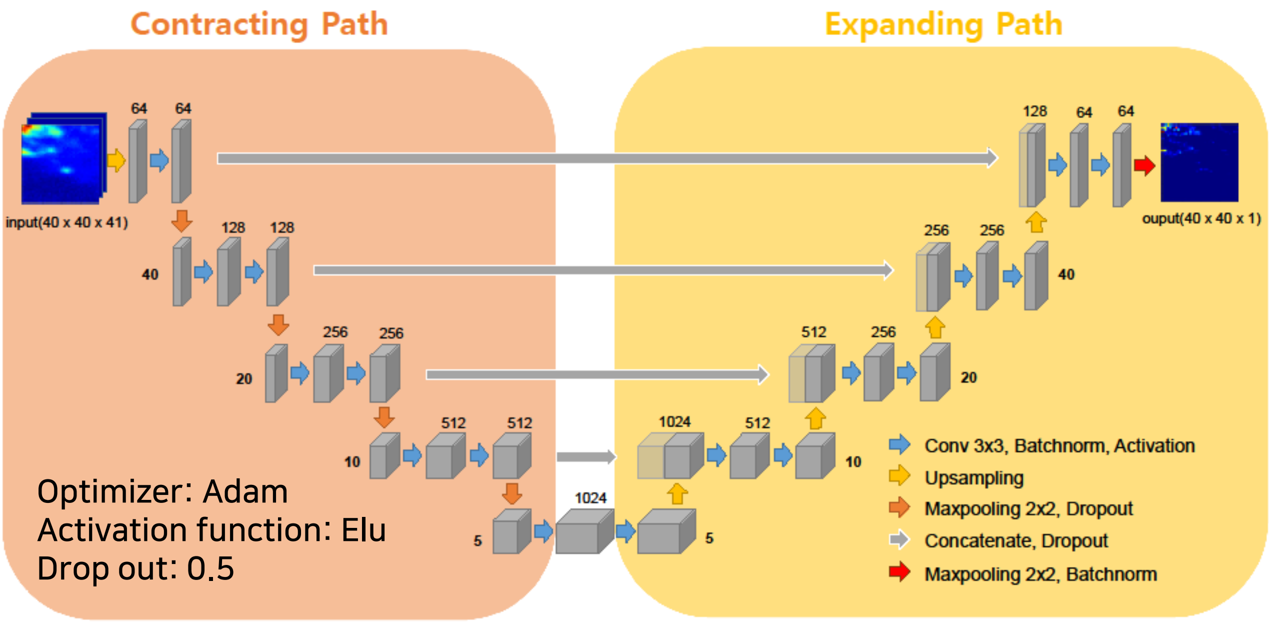

Optimizer: Adam
Activation function: Elu
Drop out: 0.5

- Training data re-sampling method using 5-fold cross validation

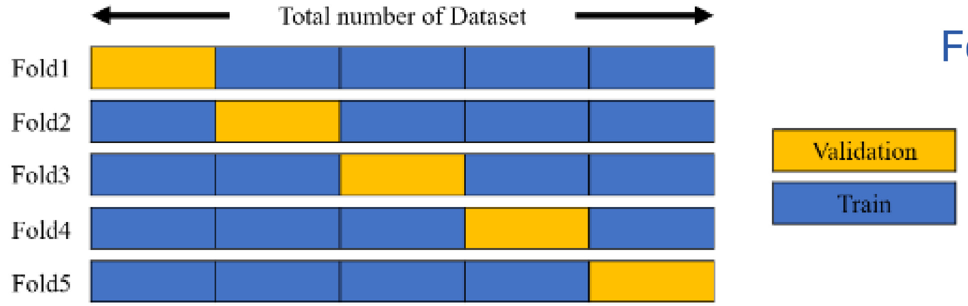

For training: Y2016-2018

- Evaluation metric

$$MAE = |true - prediction|$$:for the precipitation rate

$$F1 = 2 * \frac{Recall * Precision}{Recall + Precision}$$:for the precipitation location

$$MOF = \frac{MAE}{F1}$$

- Ensemble process for the inference step

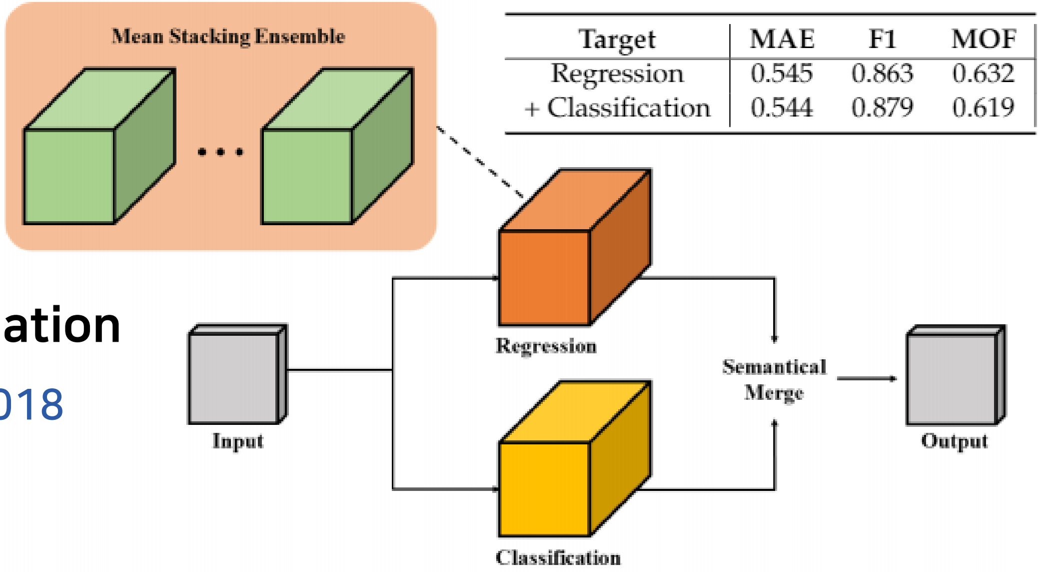

Target	MAE	F1	MOF
Regression	0.545	0.863	0.632
+ Classification	0.544	0.879	0.619

SIA

Results

GPROF(Goddard Profiling) algorithm:
GPM GMI Radiometer Precipitation Profiling L2A products

PMW-PrecipNet **GPROF**

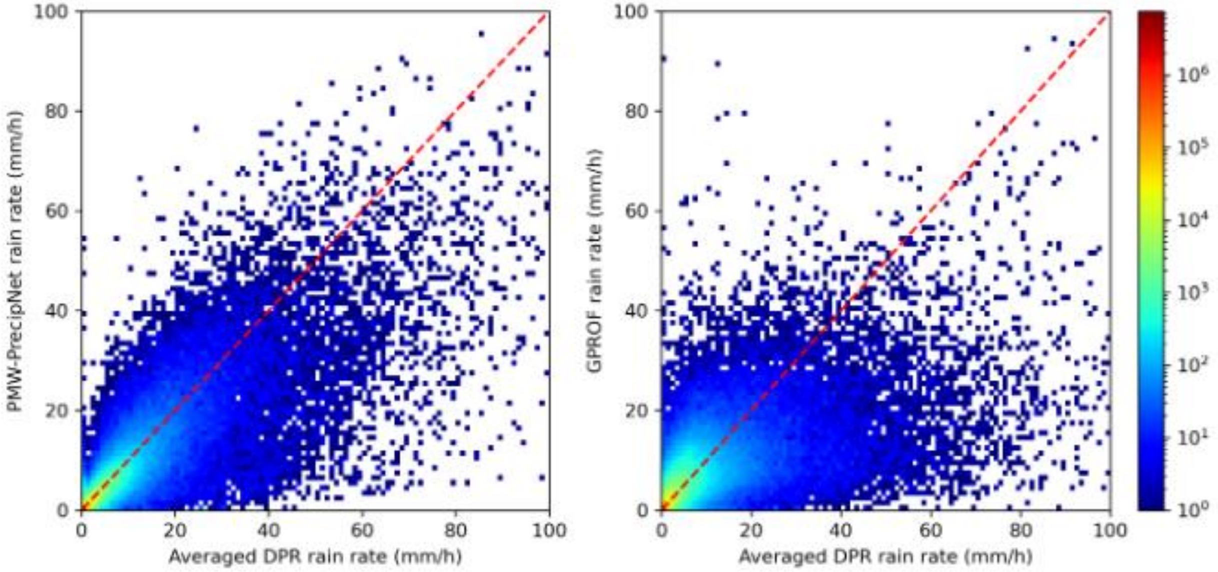

Geo. Variables	All			Ocean (85.0 %)			Land (13.5 %)			Coast (1.4 %)		
	MAE	F1	MOF	MAE	F1	MOF	MAE	F1	MOF	MAE	F1	MOF
Excluding	1.270	0.820	1.548	1.286	0.824	1.561	1.125	0.797	1.411	1.618	0.818	1.978
Including	1.258	0.824	1.528	1.275	0.827	1.542	1.110	0.803	1.383	1.608	0.821	1.960

→The performance improved the most over land among the three surface types.

R^2	Ocean	Land	Coast
PMW-PrecipNet	0.88	0.8	0.82
GPROF	0.74	0.52	0.44

PMW-PrecipNet **Averaged DPR** **DPR** **Gprof**

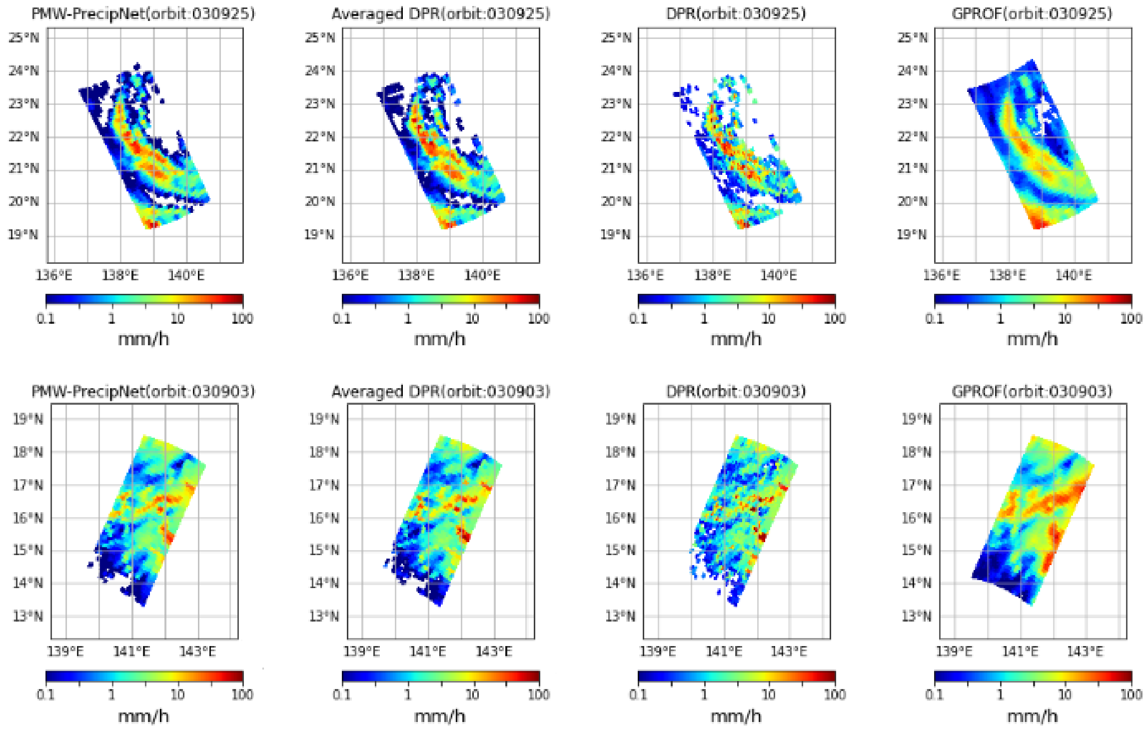

→ PMW-PrecipNET showed more detailed feature

Results

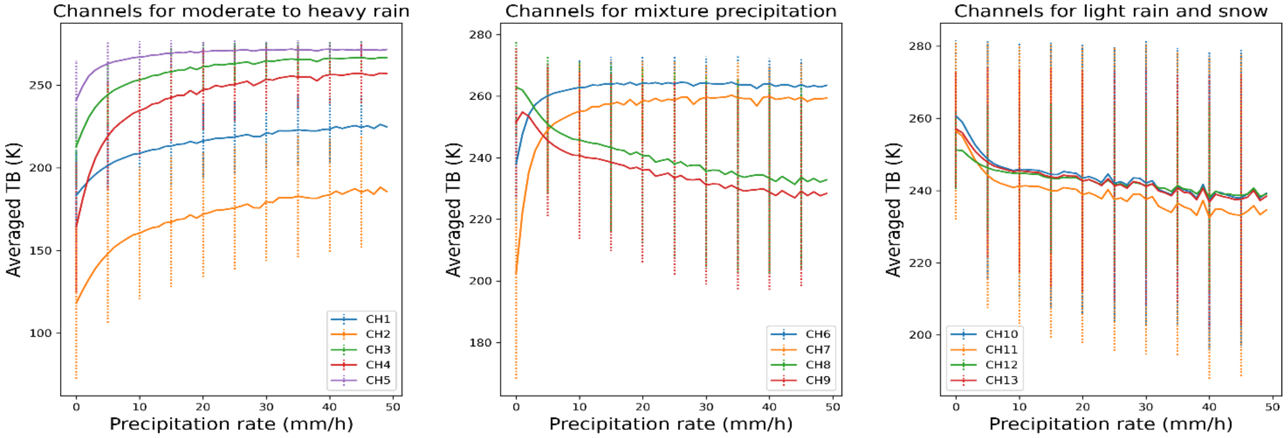

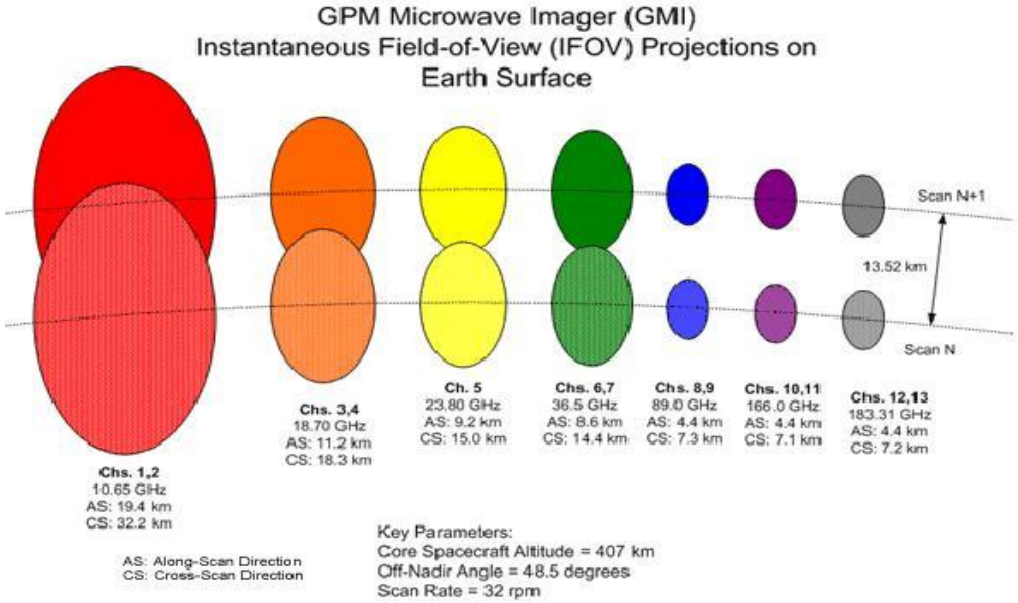

➢ Channel effect on results

Exception ch.	No exception	channel-1	channel-2	channel-3	channel-4	channel-5	channel-6	channel-7
MAE ↓	0.678	0.714	0.680	0.688	0.711	0.700	0.729	0.696
F1 ↑	0.799	0.805	0.808	0.797	0.796	0.795	0.782	0.789
MOF ↓	0.849	0.887	0.842	0.864	0.893	0.880	0.932	0.882
Exception ch.	**channel-8**	**channel-9**	**channel-10**	**channel-11**	**channel-12**	**channel-13**	**Longitude**	**Latitude**
MAE ↓	0.729	0.716	0.708	0.708	0.696	0.709	0.691	0.705
F1 ↑	0.795	0.795	0.796	0.799	0.787	0.803	0.805	0.802
MOF ↓	0.916	0.900	0.889	0.885	0.883	0.883	0.859	0.879

CH6 : the most positive impact on the results. The scattering channel is important for the rain rate accuracy.
CH 1-2: the negative impact on the precipitation location due to their lower resolution.

Conclusions

- We propose PMW-PrecipNET, a data-driven passive microwave retrieval algorithm.
- The results showed that the proposed algorithm performs well for both ocean and land surface types without the separate processes according to surface types.
- The results show that PMW-PrecipNet provides 19 % of the improved correlation with Dual Precipitation Radar compared to the operational GPM precipitation retrieval algorithm.
- This study showed the potential of a deep learning approach to retrieve precipitation without empirical engineering for constructing an a-priori database.
- For further study, we applied this method for global precipitation retrieval and examined the regional differences.

04 Precipitation forecasting

yejichoi@si-analytics.ai

HPC Cluster-based User-defined Data Integration Platform for Deep Learning in Geoscience Applications (submitted in computers and geoscience journal)

- GEO-DIP architecture

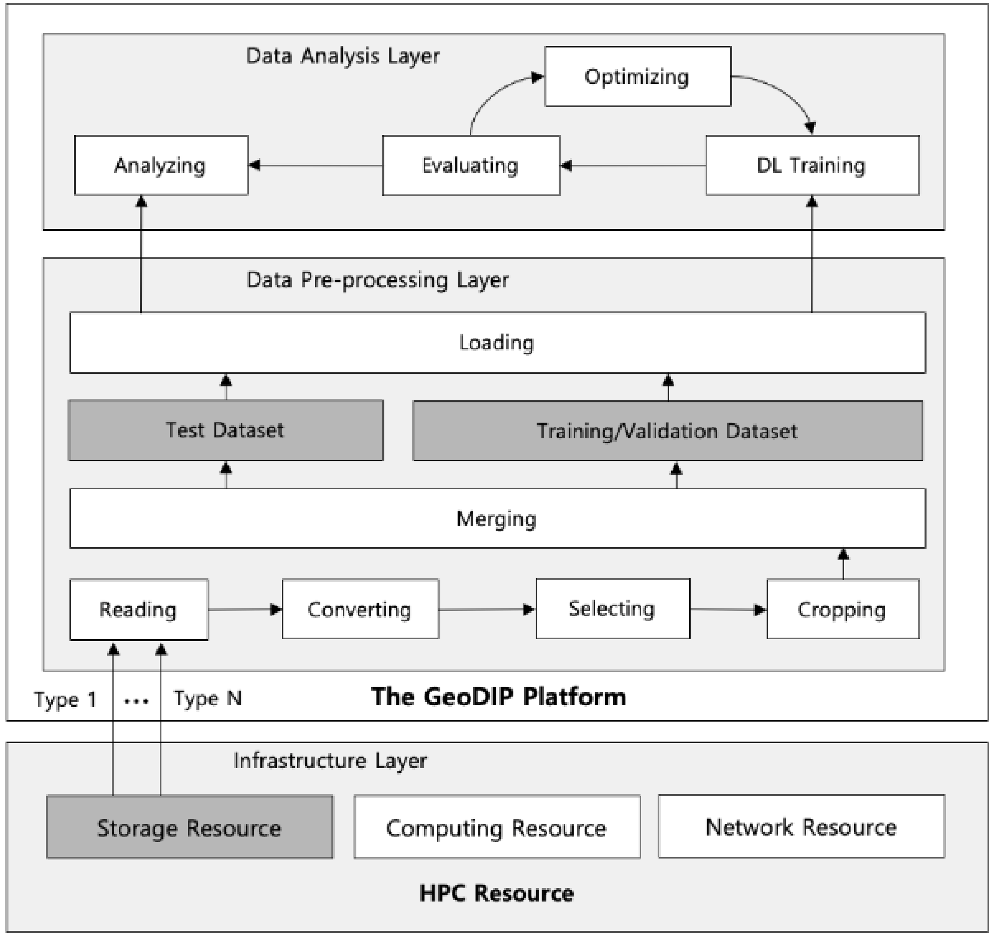

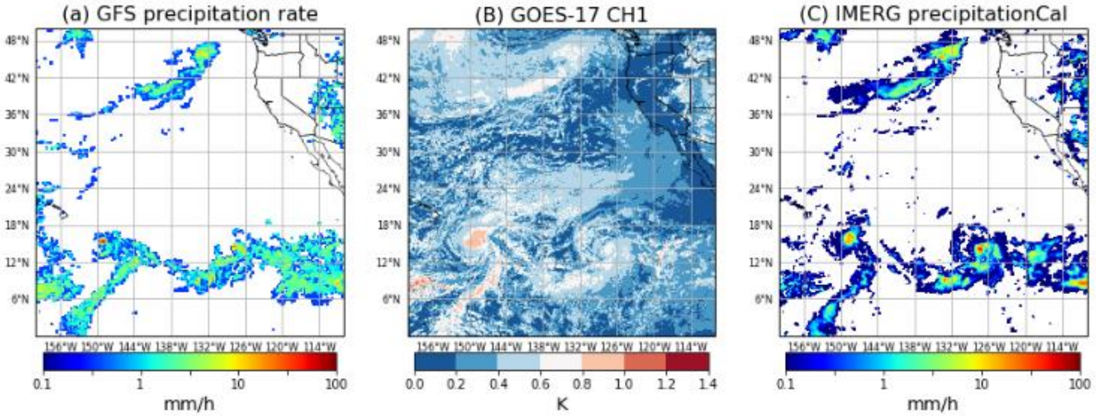

Table 4
Precipitation prediction results for after one hour of each experiment depending on the number of datasets for the training process

Number of data source	Data set	Precision		Recall		F-score	
		No Rain	Rain	No Rain	Rain	No Rain	Rain
3 data sources	GOES-17+IMERG+GFS	0.988	0.795	0.993	0.693	0.991	0.741
2 data sources	GOES-17+IMERG	0.989	0.771	0.992	0.712	0.990	0.740
	GFS+IMERG	0.988	0.780	0.993	0.689	0.990	0.732
	GOES-17+GFS	0.977	0.726	0.994	0.389	0.986	0.507
1 data sources	IMERG	0.988	0.789	0.993	0.672	0.990	0.726
	GOES-17	0.982	0.625	0.988	0.523	0.985	0.569

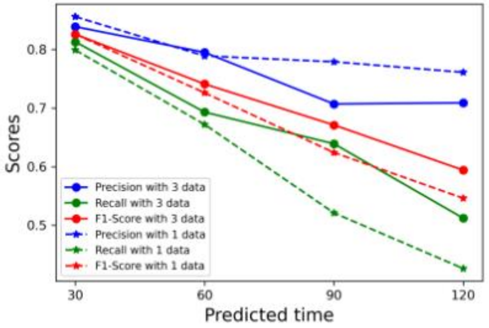

Figure 7: The result scores over predicted time depending on the number of training data set

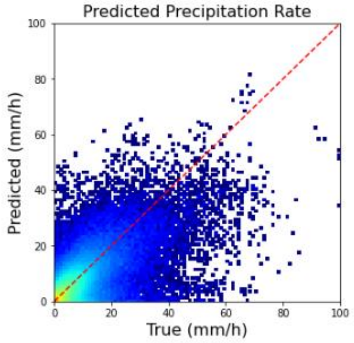

Figure 8: The scatter plots of true and predicted precipitation rate after one hour

Heavy rainfall prediction from satellite and radar observations

- The results with only radar data can not predict the heavy rainfall development and extinction and the heavy rainfall region is much wider than the true.
- The results with radar and Himawari data together show similar patterns and follow well to precipitation system development

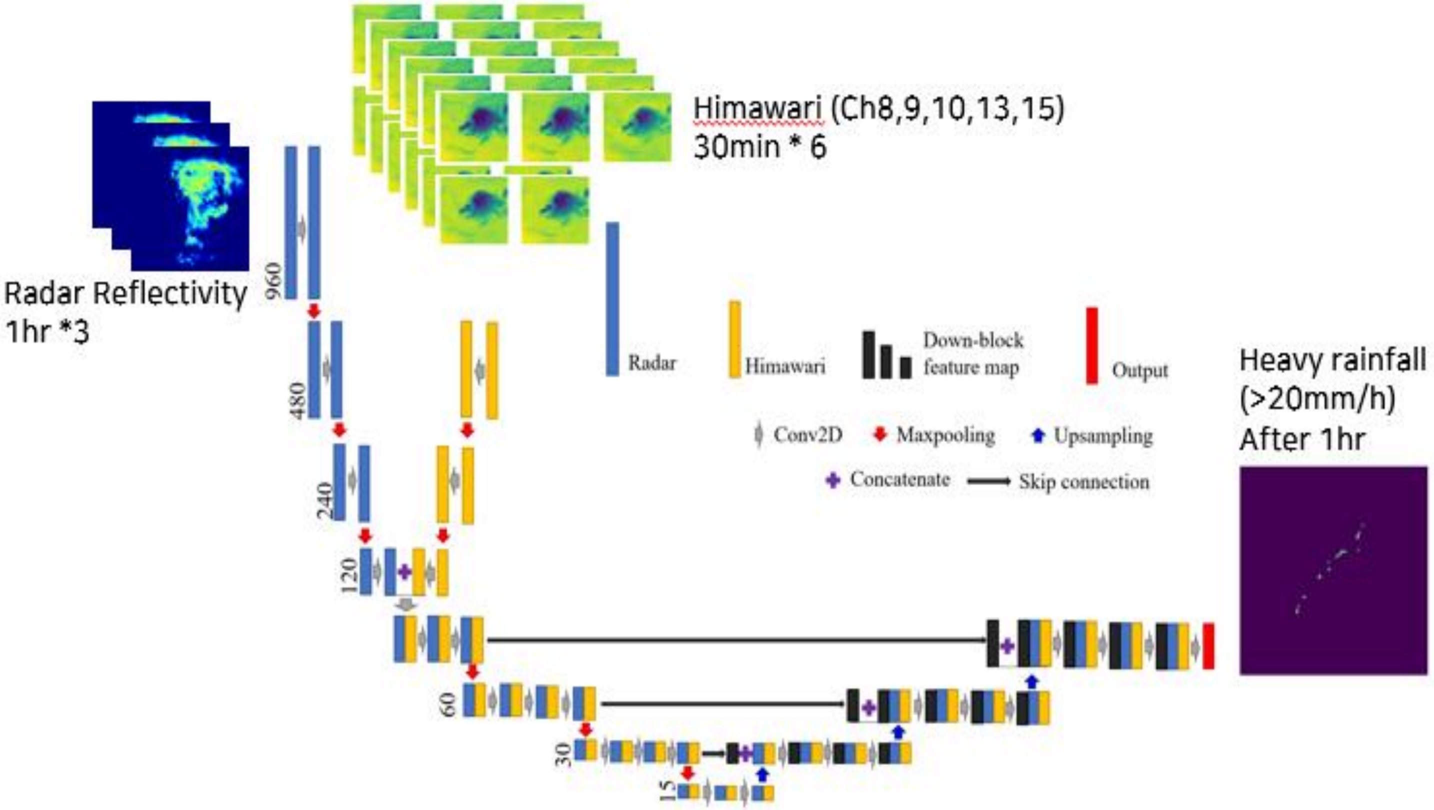

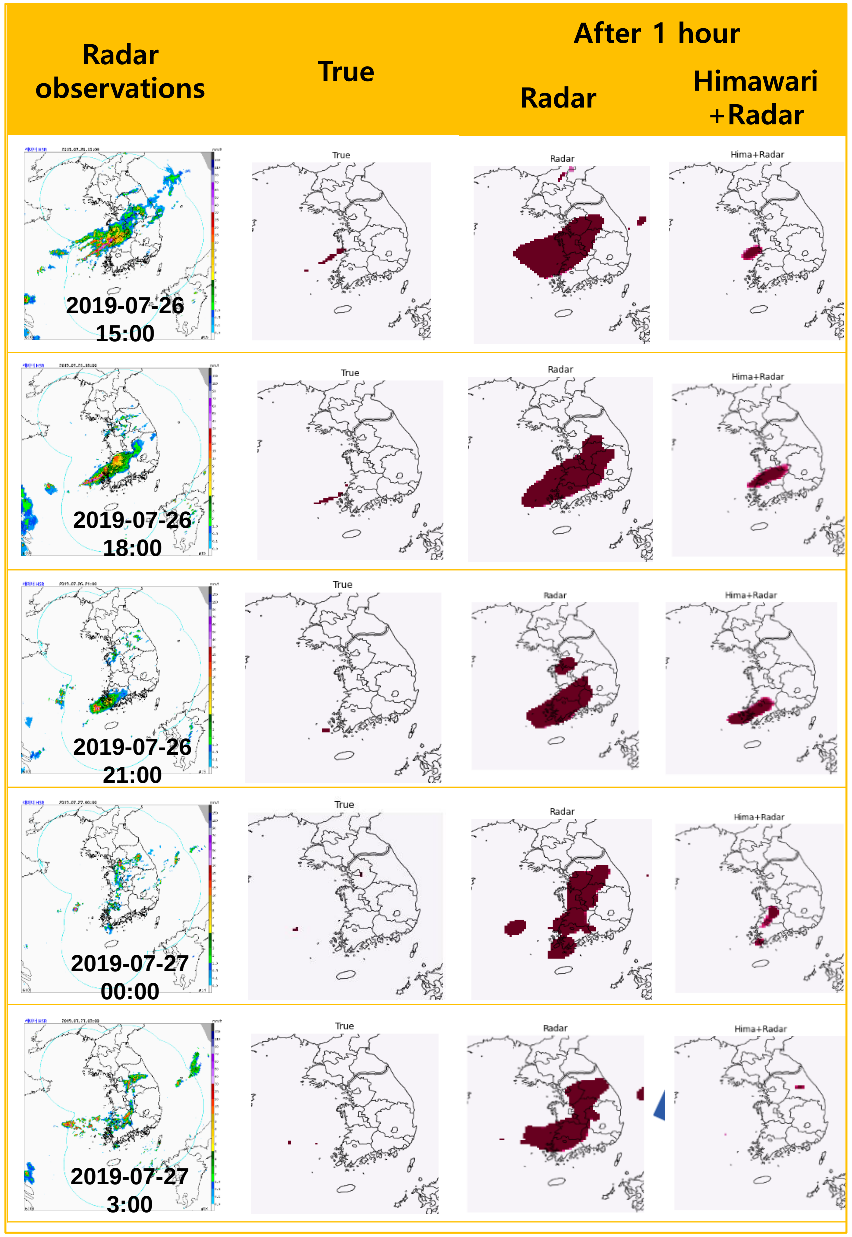

Take home message

- Recently, deep learning techniques are increasingly used in the weather and climate community with various applications.
- Earth system data can be considered ‘big data,’ and we should consider how to prepare ‘AI-ready data’ using ‘big earth data.’
- There is a various observed data type for the same atmospheric phenomenon from multiple sources.
    - Temporal and spatial resolution and coverage
    - The physical relations between different atmospheric variables
    - The observation characteristics (Indirect/direct, instantaneous/cumulative)
- When the supervised learning method is adopted, we should carefully consider which data can be a ground truth and the quality evaluation.
- The high-resolution weather and climate data need big memory in the training process; we need to solve GPU memory limitations. For this, domain scientists and machine learning/computer scientists should collaborate.

SIA

주식회사 에스아이에이
SI ANALYTICS

Thank you for attention

www.si-analytics.ai

SI Analytics Co., Ltd. (Satrec Initiative Group)
441Expo-ro, Yuseong-gu, Daejeon, 34051, Korea

yejichoi@si-analytics.ai